Strain-induced birefringence in GaAs

James E. Raynolds,* Zachary H. Levine,† and John W. Wilkins
Department of Physics, The Ohio State University, Columbus, Ohio 43210-1106
(Received 23 November 1994)

We present the results of density-functional calculations of the dielectric function and the photoelastic tensor—the susceptibility for strain-induced birefringence—in GaAs for photon frequencies below the direct band gap. These calculations were performed in the Kohn-Sham local-density approximation in a pseudopotential/plane-wave scheme which includes local-field effects and self-energy corrections. We find that traditional special-points integration methods are inadequate for performing the Brillouin-zone integrals involved in computing the photoelastic tensor. Very high resolution of the critical point at $k=0$ is needed to obtain even the correct *qualitative* behavior of the photoelastic tensor. Accurate expansions of the integrand in spherical harmonics for small k and plane waves elsewhere in the Brillouin zone were obtained and an integration approach which correctly integrates the expansions was used. Dramatic improvement in the qualitative frequency dispersion of the photoelastic tensor, in comparison with experiments, is obtained despite a large (50%) shift of the static value away from the measurement. We also present the result of a calculation of the internal strain relaxation associated with strains along the bonding [111] direction. These results are in excellent agreement with two previous *ab initio* calculations and with recent measurements.

I. INTRODUCTION

Strain-induced optical and transport properties in semiconductors are currently of interest for their relevance to the design and characterization of electronic and optoelectronic devices which often, by construction, contain built-in strain.[1] Osbourn greatly widened the selection of materials to be used in the construction of devices based on semiconductor heterojunctions by demonstrating that substantial lattice mismatch between the constituent materials can be accommodated without the formation of dislocations if the layers comprising the junction are sufficiently thin.[2] The resulting strain alters the electronic structure of the materials forming the junction and as such offers the experimentalist the opportunity to tune the electronic properties of the devices for specific applications. For example, Temkin *et al.* introduced a Si-based photodiode which had its absorption edge strain shifted to the 1.3–1.5-μm window of optical fibers used by the telecommunication industry.[3] Strained heterojunction devices are also of fundamental interest since often they are so small—layer thickness on the order nanometers—that quantum-size effects are important.[1] In order to fully understand the interrelation between strain effects and quantum-size effects, an understanding of strain in bulk semiconductors is essential.

Ab initio calculations of optical properties of semiconductors, and in particular the dielectric function,[4–15] are also currently of fundamental interest with regard to issues concerning improvements to the density-functional theory of electronic structure.[16,17] Density-functional theory[18] in the local-density approximation[19] (LDA), which has become the standard method for parameter-free calculations in solids, yields accurate results for many properties of atoms, molecules, insulators, semiconductors, and metals,[20–22] but fails for the static dielectric function in semiconductors.[23–25] Results obtained using the LDA are consistently overestimated; discrepancies with experiments are typically between 10% and 20%.[4] Levine and Allan's quasiparticle theory of optical response is based on the assumption that the overestimate of the dielectric function is due to a related failure of the LDA: the underestimate of band gaps in semiconductors.[4] Their theory corrects the LDA band gap with a rigid upward shift of the conduction bands (and a corresponding renormalization of the momentum operator) and leads to agreement with experiment to within a few percent. Other recent attempts to go beyond the LDA include the use of gradient-corrected functionals[16] and the suggestion that density-functional theory should be reformulated to explicitly include electronic polarization.[17]

The focus of the present work is the first-principles calculation of the photoelastic tensor[26,27]—the susceptibility describing changes in the dielectric tensor induced to linear order by an applied strain—for photon energies below the fundamental band gap in bulk GaAs. These calculations are based on Levine and Allan's quasiparticle theory of optical response.[4] The dielectric function is calculated for the crystal in the presence of small strains, and the eigenvalues of the photoelastic tensor are obtained by taking finite differences of the dielectric function in the strained and unstrained crystals. This theory has been previously applied successfully to the calculation of the photoelastic tensor in Si.[28] While excellent results—agreement with experiment to within a few percent—are obtained for the dielectric function using a standard 60-point k-space integration method,[4] the photoelastic tensor in GaAs required an integration technique to confront Brillouin-zone integrals over functions which (1) oscillate between positive and negative values, leading to substantial cancellation; and (2) receive large contributions from a very small volume near the point

0163-1829/95/51(16)/10477(12)/$06.00

$k=0$ (the Γ point) in k space. The frequency dispersion of the photoelastic tensor is extremely sensitive to the treatment of these integrals to the extent that not even the correct qualitative dispersion is obtained when the 60-point mesh is used. The method leads to greatly improved qualitative results for the frequency dispersion of the photoelastic tensor, as well as a 50% correction to the static $p_{12}-p_{11}$ component of the photoelastic tensor compared to results obtained using the 60-point integration method. Unfortunately the improvement of the dispersion is only qualitatively better and the 50% correction worsens the static value. These results do, however, demonstrate that details of the integration technique are very important, and suggests that effects beyond those included in our theory, such as spin-orbit and particle-hole interactions, are far more important for the photoelastic effect than they are for the dielectric function.

The frequency dispersion of the p_{44} eigenvalue of the photoelastic tensor in Si was found, in a previous calculation, to be extremely sensitive to the degree of structural relaxation in the presence of a strain along the [111] direction.[28] Accordingly we have performed a careful calculation of the internal strain relaxation using total-energy minimization.

II. CALCULATION

The ground-state band structure is solved using the local-density approximation (LDA) in a pseudopotential/plane-wave basis using the program of Allan and Teter.[29,30] A 10-Hartree energy cutoff was used for the plane-wave expansion, and Hamann's norm-conserving pseudopotentials[31] in the Kleinmann-Bylander separable form[32] were used. For the exchange-correlation functional, we used Teter's parametrization[33] of the Ceperley-Alder exchange-correlation data.[34] Ten special k points[35,36] were used to perform the Brillouin-zone integrals involved in obtaining the ground-state self-consistent potential. The frequency-dependent dielectric function was then obtained from the ground-state energies and wave functions using Levine and Allan's quasiparticle formulation of optical response.[4] In this theory the LDA Hamiltonian is modified as

$$H_{\mathbf{k}}=H_{\mathbf{k}}^{\mathrm{LDA}}+\Delta_{\mathbf{k}}P_{c\mathbf{k}} , \tag{1}$$

where the second term is a self-energy correction, $\Delta_{\mathbf{k}}$ is an energy shift, and $P_{c\mathbf{k}}$ is the projection operator for the conduction states. In practice we ignore the slight k dependence of the energy shift [0.2 eV in GaAs (Ref. 25)], and take $\Delta=0.8$ eV as suggested by GW calculations.[25] Local-field corrections are also included in our calculations.[4,37]

Changes in the dielectric function resulting from small applied strains are quantified by the following relation:

$$\delta\varepsilon_{ij}^{-1}=p_{ijkl}\mu_{kl} , \tag{2}$$

where μ_{kl} is the strain, ε_{ij}^{-1} is the inverse dielectric function, and p_{ijkl} is the photoelastic tensor.[26] Repeated indices in Eq. (2) are to be summed. The photoelastic tensor is a fourth-rank tensor symmetric in the pairs of indices $\{ij\}$ and $\{kl\}$ since it relates two symmetric second-rank tensors. There are only three independent components of the photoelastic tensor in cubic crystals: p_{1111}, p_{1122}, and p_{2323}.[26] In what follows we will use the compressed notation:[28,38,39] $11\rightarrow1$, $22\rightarrow2$, $33\rightarrow3$, $23\rightarrow4$, $13\rightarrow5$, and $12\rightarrow6$.

The three eigenvalues of the photoelastic tensor are $p_{11}+2p_{12}$, $p_{11}-p_{12}$, and p_{44}, which correspond to the strain eigenvectors: uniform volume change, tetragonal shear strain, and trigonal shear strain, respectively. Simple expressions for the various eigenvalues of the photoelastic tensor in terms of strain-induced changes in the dielectric function follow from Eq. (2), and have been derived in Ref. 28. The results are

$$p_{11}+p_{12}=\frac{\varepsilon_0-\varepsilon}{\varepsilon_0^2(\delta a/a)} , \tag{3}$$

$$p_{12}-p_{11}=\frac{\varepsilon_{\parallel}-\varepsilon_{\perp}}{\varepsilon_0^2(\delta l/l)} , \tag{4}$$

and

$$p_{44}=\frac{\varepsilon_{\parallel}-\varepsilon_{\perp}}{2\varepsilon_0^2(\delta l/l)} . \tag{5}$$

In the above equations ε and ε_0 denote the dielectric function in the strained and unstrained crystals, respectively. The quantities $\varepsilon_{\parallel}$ and $\varepsilon_{\perp}$ are the components of the dielectric function in the strained crystal associated with light polarized in directions parallel and perpendicular to the strain axis, respectively. In Eq. (3), $\delta a/a$ is the change in lattice constant and $\delta l/l$ in Eqs. (4) and (5) is the change in length measured along the strain directions. For readers who wish to compare the above equations with those of Ref. 28, please be aware that Eqs. (4) and (5) correspond to shear strains—that is, volume-conserving strains—whereas volume-nonconserving strains were employed in the work of Ref. 28.

Calculation of the photoelastic tensor for bulk GaAs proceeds by calculating the frequency-dependent dielectric function for the unstrained crystal, at the experimental lattice constant ($a=0.5498$ nm), as well as the crystal strained in the three ways mentioned above: (1) symmetry-preserving volume changes, (2) the tetragonal shear strain (i.e., the volume-conserving strain along the [001] axis), and (3) the trigonal shear strain (i.e., the volume-conserving strain along the [111] axis). The finite differences indicated in Eqs. (3), (4), and (5) are then applied to the calculated quantities to yield the eigenvalues of the photoelastic tensor. We use very small strains—$\delta a/a=0.0004$—which correspond to a stress of roughly 10^8 dyn/cm^2 which is well within the linear regime of the experiments.[40]

In the present study it was found that, unlike the dielectric function, the photoelastic tensor in GaAs is extremely sensitive to the sampling of the critical point at $\mathbf{k}=0$ (the Γ point), demanding the use of a sophisticated integration technique which succeeds where traditional special-points methods fail. The dielectric function[4] and the photoelastic tensors are obtained in terms of

Brillouin-zone integrals—the integrals for the latter being given simply in terms of differences of the former [as indicated by Eqs. (3)–(5)]. The integrands associated with the static dielectric constant and the $p_{12}-p_{11}$ component of the photoelastic tensor are plotted in Fig. 1 as functions of $\mathbf{k}$ along the [111] direction in k space. In the units of this figure, the zone edge (the L point) is at $k=0.886$ (not shown). Along other directions in k space, similar behavior is observed. Also indicated in the figure are the two sampling points nearest to $k=0$ when a 60-point special k-point mesh [Monkhorst and Pack's (8,8,8) mesh (Ref. 35)] is used; these are indicated by the upward-pointing triangles. The downward-pointing triangles indicate the corresponding points when a 110-point special-points mesh [Monkhorst and Pack's (10,10,10) mesh (Ref. 35)] is used. We see that both of the integrands shown are strongly peaked near $k=0$, and that neither of the special-points meshes are capable of correctly sampling these peaks.

What is not obvious from Fig. 1 is that the situation is drastically worse for the photoelastic tensor. In the case of the dielectric function, the peak near the Γ point represents only a very small correction, and the 60-point mesh gives accurate results. For the photoelastic tensor, the integration of the peak at Γ represents a 50% correction to results obtained using the 60-point mesh (to be verified in Sec. III). For the frequency-dependent photoelastic tensor the difficulties near Γ become increasingly more severe with increasing photon frequency, and the integrand becomes singular at the direct band gap.

In addition to the radial dependence indicated in Fig. 1, the integrand contains considerable oscillation between positive and negative values as a function of the direction of $\hat{k}$. This dependence is conveniently quantified by expanding in spherical harmonics as

$$P(\mathbf{k})=\sum_{l,m} C_{l,m}(k)Y_{l,m}(\theta,\phi)\ , \tag{6}$$

where the radial dependence is included through the k dependence of the expansion coefficients $C_{l,m}(k)$, and the function $P(\mathbf{k})$ is understood to be the integrand which is being expanded. The expansion coefficients were obtained for a set of k values by numerically evaluating the projection integral

$$C_{l,m}(k)=\int d\Omega\ Y^*_{l,m}(\theta,\phi)P(k,\theta,\phi) \tag{7}$$

on a spherical mesh of radius k constructed to exactly integrate the orthogonality relation

$$\int d\Omega\ Y^*_{l,m}(\theta,\phi)Y_{l',m'}(\theta,\phi)=\delta_{l,l'}\delta_{m,m'}\ , \tag{8}$$

for all l and l' up to some maximum which depends on the area density of points of the sampling mesh.[41] In the above equations, the coordinates (k,θ,ϕ) are the spherical-polar coordinates of the vector $\mathbf{k}$, and $d\Omega$ is the differential of solid angle. The first eight $m=0$ spherical-harmonic coefficients, $C_{l,0}(k)$, for the photoelastic integrand are plotted in Fig. 2 as functions of k. The

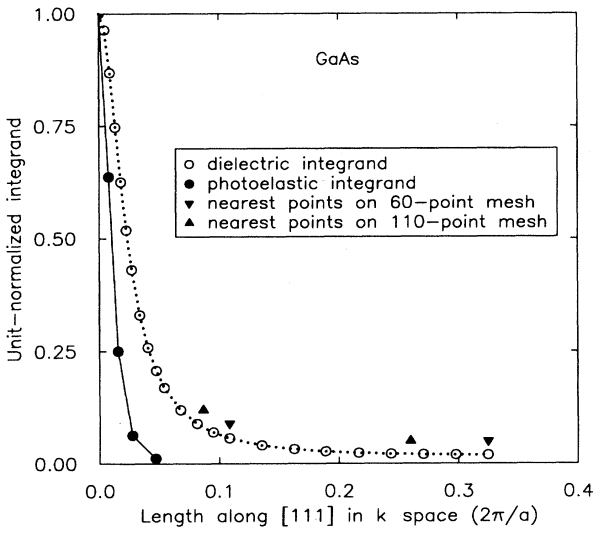

FIG. 1. Integrands for the unstrained dielectric function and the $p_{12}-p_{11}$ component of the photoelastic tensor plotted as functions of k along the [111] direction in k space, each exhibiting a peak at $k=0$. The curves are normalized to unity at $k=0$. The positions of the nearest two mesh points of a 60-point mesh and on a 110-point mesh are indicated by the black triangles, demonstrating that the 60- and 110-point meshes completely miss the peaks. The integrand for the photoelastic tensor has a similar shape to the one for the unstrained dielectric function, but the ratio of the $k=0$ value to that at the first mesh point is an order of magnitude larger than for the dielectric function. Numbers of special points refer to the irreducible zone in full cubic symmetry.

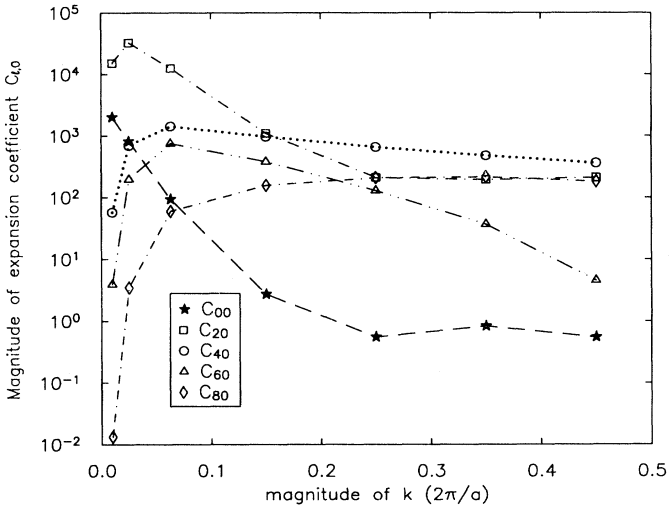

FIG. 2. Spherical-harmonic expansion coefficients $C_{l0}(k)$ for the integrand associated with the long-wave, static $p_{12}-p_{11}$ component of the photoelastic tensor for $l=0$–8 as functions of k. All C_{lm} with the same l have similar behavior. The only term which contributes to the integral, i.e., C_{00}, is at least an order of magnitude smaller than the higher harmonics at all but the smallest values of k (not shown). A uniform mesh will have difficulty capturing the C_{00} contribution accurately. All harmonics except C_{00} vanish in the limit $k\rightarrow 0$ at least as fast as k^2, while C_{00} goes to a constant (Ref. 44).

oscillatory components are at least one to two orders of magnitude larger than $C_{00}(k)$ (and thus the angular average).

Special-points methods based on the Monkhorst-Pack scheme[35] (uniform meshes of k points) imply a Fourier interpolation of the sampled integrand. This simply means that the sampled function can be written as a plane-wave expansion which is exactly integrated by the special points. More explicitly, if we expand an arbitrary k-space function $P(\mathbf{k})$ as

$$P(\mathbf{k})=\frac{1}{N}\sum_{p} C_p e^{i\mathbf{k}\cdot\mathbf{R}_p} , \tag{9}$$

then the discrete orthogonality relation

$$\sum_{\mathbf{k}_j} (e^{i\mathbf{k}_j\cdot\mathbf{R}_p})^* e^{i\mathbf{k}_j\cdot\mathbf{R}_q}=N\delta_{pq} \tag{10}$$

is satisfied, when evaluated on a uniform mesh of k points $\mathbf{k}_j$, for all p and q up to some maximum value. In Eq. (10), N is the number of k points and the $\mathbf{R}$'s are direct-space lattice vectors which are simply used here as formal expansion parameters and have no further physical significance. The expansion coefficients C_p in Eq. (9) can be evaluated in terms of the sampled integrand by using Eq. (10) to project an approximation $\tilde{C}_p$ as

$$\tilde{C}_p \approx \sum_{\mathbf{k}_j} (e^{i\mathbf{k}_j\cdot\mathbf{R}_p})^* P(\mathbf{k}_j) . \tag{11}$$

If the sampling mesh is chosen to be sufficiently dense such that Eq. (10) is satisfied for all p in the expansion of Eq. (9), then Eq. (11) exactly gives the expansion coefficients C_p.

By substituting the approximate expansion coefficients $\tilde{C}_p$ into the plane-wave expansion of Eq. (9), we obtain an approximation $\tilde{P}(\mathbf{k})$ to the desired function $P(\mathbf{k})$ at any arbitrary $\mathbf{k}$ based on the known values $P(\mathbf{k}_j)$ on the sampling mesh. We say that the function $\tilde{P}(\mathbf{k})$ is obtained by Fourier interpolation from the values on the sampling mesh.[42] The function $\tilde{P}(\mathbf{k})$ is used in what follows to ascertain the effectiveness of the uniform integration mesh for various regions of the Brillouin zone.

A. The Γ-point region

Outside of a small spherical region centered around $k=0$ which occupies roughly 2% of the zone volume, the integrand is well represented by a plane-wave expansion and can thus be accurately integrated using a sufficiently dense uniform mesh of k points. Inside the spherical region only $C_{00}(k)$ leads to a nonvanishing contribution to the volume integral of $P(\mathbf{k})$. Since the $C_{00}(k)$ component is proportional to the spherical average of $P(\mathbf{k})$ over a sphere of radius k, we define the radial function $\rho(k)$ as

$$\rho(k)=\frac{\sqrt{4\pi}k^2 C_{0,0}(k)}{V_{\mathrm{BZ}}} , \tag{12}$$

where V_{BZ} is the Brillouin-zone volume. We then write the three-dimensional integral of $P(\mathbf{k})$ over the volume of a sphere of radius k_{sphere} in terms of a one-dimensional integral over the radial function:

$$\frac{1}{V_{\mathrm{BZ}}}\int_{V_{\mathrm{sphere}}} d^3k\, P(\mathbf{k})=\int_0^{k_{\mathrm{sphere}}} dk\, \rho(k) . \tag{13}$$

The radial function $\rho(k)$ and two approximate radial functions $\tilde{\rho}(k)$ [defined with $\tilde{C}_{00}(k)$ substituted for $C_{00}(k)$ in Eq. (12)] obtained using Fourier interpolation from two uniform meshes—one more dense than the other—are plotted in the lower panel of Fig. 3. When the lower-density uniform mesh is used, agreement between $\rho(k)$ and $\tilde{\rho}(k)$ is obtained for $k>0.35(2\pi/a)$. When the more dense uniform mesh is used, agreement is obtained for $k>0.2(2\pi/a)$.

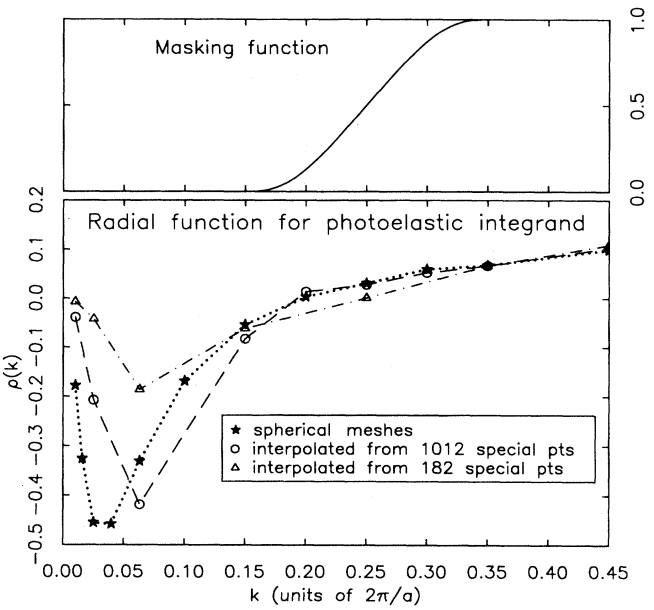

FIG. 3. Masking function $\xi(k)$ [upper panel, Eq. (15)] and converged radial function [lower panel, Eq. (12)] for the integrand associated with the static $p_{12}-p_{11}$ component of the photoelastic tensor neglecting local fields, compared with two approximate radial functions. Agreement between the converged and approximate radial functions in the region not plotted—out to the zone edge at the L point [$k=0.886(2\pi/a)$ in these units]—is better than 99%. For a given approximate radial function, the number given in the legend is the equivalent number of points in the irreducible Brillouin zone for full cubic symmetry of the uniform mesh used to construct the Fourier-interpolated radial function. For the higher-density uniform mesh (1012 points in the irreducible zone) the exact and approximate radial functions match for $k>0.2$ (units of $2\pi/a$) and for the lower-density uniform mesh (182 points in the irreducible zone) for $k>0.35$.

B. Two-mesh integration technique

Our integration method employs a hybrid description in which the small-k region is represented by spherical-harmonic expansions, and the rest of the zone is represented by plane-wave expansions, with a smooth transition between the two descriptions provided by a masking function $\xi(k)$. In other words, we write the k-space volume integral of $P(\mathbf{k})$ as

$$\int d^3k\, P(\mathbf{k}) = \int d^3k\, P(\mathbf{k})\xi(k) + \int d^3k\, P(\mathbf{k})[1-\xi(k)]\,, \tag{14}$$

where we have simply added and subtracted the integrals involving the masking function $\xi(k)$. The first integral on the right side of Eq. (14) is evaluated on a uniform mesh of k points (special points), and the second term is evaluated on concentric spherical meshes (with appropriately chosen weights) which were used to project the radial functions of Fig. 3. The function $\xi(k)$ was chosen to smoothly go from 0 to 1 in some range $k' \le k \le k''$, which is chosen such that for $k > k''$ the integrand is smooth enough to be integrated using the special points and for $k < k'$ the integrand is more efficiently integrated on the spherical-shell meshes. For $k' \le k \le k''$ both descriptions must be adequate. The function $\xi(k)$ is plotted in the top panel of Fig. 3 and is defined as[43]

$$\xi(k) = \frac{1}{2}\left[1+\tanh\left[\frac{bx}{1-x^2}\right]\right], \tag{15}$$

where x goes linearly from -1 to 1 in the range from $k' \le k \le k''$. For $k \le k'$, $\xi(k)=0$, and for $k \ge k''$ $\xi(k)=1$. The results are almost completely insensitive to the choice of b in the range $0.05 \le b \le 20$.[44]

Ultimately we wish to have an integration method which requires the smallest number of points. It is more difficult to converge the radial function by directly sampling with the spherical meshes as we go to progressively larger k. For this reason, the extra computational expense involved in using 1012 special points instead of, say, 182 is offset by the savings of needing fewer spherical meshes. The method used to produce all results is based on the use of 1012 special points, which uniformly span the irreducible Brillouin zone, in conjunction with 11 spherical shells, at the k radii indicated in Fig. 3, each having 80 points on the shell section in the irreducible Brillouin zone, plus one point at $k=0$, for a total of 1893 points in the irreducible zone.[45,46]

The degree of difficulty in integrating the small region near $k=0$ is exemplified by the fact that we need 881 points to span this region, which accounts for roughly 2% of the zone volume (as determined by performing a volume integral over the masking function and dividing by the total zone volume) as compared with the rest of the zone which is adequately sampled by 1012 special points. As we will see, order-1 corrections come from the small region surrounding $k=0$.

C. Why 80 points on each spherical shell?

The radial function $\rho(k)$ is obtained at each k from the $C_{00}(k)$ coefficient of the spherical-harmonic expansion, the expansion of which is judged to be converged when enough terms have been included such that the coefficients C_{lm} with the largest values of l are smaller than C_{00} by a factor of 10. The behavior of the expansion coefficients C_{l0} as a function of l is plotted in Fig. 4 for three characteristic values of k: 0.01, 0.25, and 0.45 (in units of $2\pi/a$). These values—the smallest value used in the calculation of $\rho(k)$, the midpoint of the matching region, and a point beyond the larger endpoint of the matching region, respectively—typify the convergence of Eq. (6). Higher l are needed to converge the expansion for larger k. For example, the curve for $k=0.25$ was obtained with 80 sphere points in the irreducible cubic Brillouin zone, whereas 624 points were needed to obtain the curve for $k=0.45$. Fortunately, it was found that the error incurred when using the 80-point mesh to obtain $C_{00}(k=0.45)$, rather than using the 624-point mesh, was quite small, on the order of 1%. Similar accuracy was obtained for all $C_{00}(k)$ with $k<0.45$ using the 80-point mesh. For this reason, the 80-point meshes were judged to be sufficiently accurate to converge the radial function for all k used to define the Γ-point region, as described in the preceding paragraphs. The $\Delta l = 10$ periodicity observed in $C_{l0}(k=0.45)$ in Fig. 4 is unexplained. An in-depth description of the calculational procedures and results can be found elsewhere.[44]

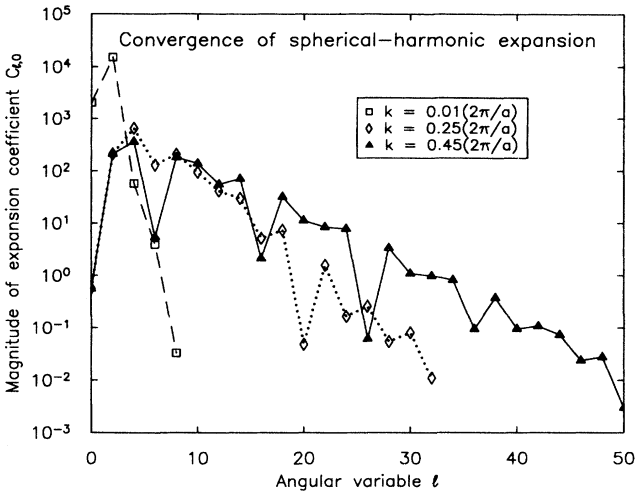

FIG. 4. Spherical-harmonic coefficient C_{l0}, for the expansion of the integrand associated with the static $p_{12}-p_{11}$ component of the photoelastic tensor, at three radii in k space: $k=0.01(2\pi/a)$ (the smallest spherical mesh radius), $0.25(2\pi/a)$ (the midpoint of the matching region), and $0.45(2\pi/a)$ (largest radius used for computing the radial function), plotted as a function of l. For each radius, the expansion is considered to be converged when the magnitude of the coefficient with highest values of l is at least an order of magnitude smaller than the C_{00} coefficient. For the smallest value of k, the expansion is well converged by $l=8$. To converge the expansion for $k=0.25(2\pi/a)$ and $0.45(2\pi/a)$ requires $l=30$ and 50, respectively.

III. RESULTS

Results for the photoelastic tensor obtained using the two-mesh integration technique, compared with results obtained using the special-points method, show a dramatic improvement in the frequency dispersion of the photoelastic tensor as well as a large correction to one of its static components. Comparison with experimental results, also shown in Figs. 5–7, will be discussed in Sec. IV. Results for the $p_{12}-p_{11}$ component are plotted in

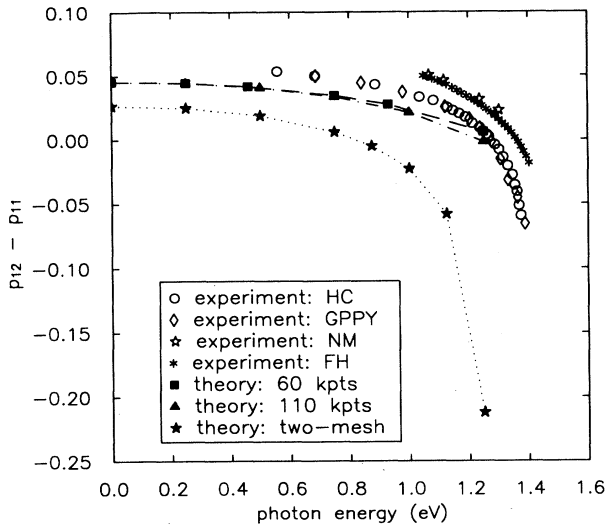

FIG. 5. Best results (two-mesh method) for the frequency-dependent $p_{12}-p_{11}$ component of the photoelastic tensor compared with four sets of experimental results and contrasted with the results obtained using uniform 60 and 110 k-point meshes. Local-field corrections are included. The near-Γ-point contributions lead to a large correction to the static value as well as greatly enhanced dispersion. Note that the similarity between the 60- and 110-point results would ordinarily lead one to conclude that convergence had been reached. The experimental references are as follows: HC (Ref. 40), GPPY (Ref. 64), NM (Ref. 65), and FH (Ref. 66).

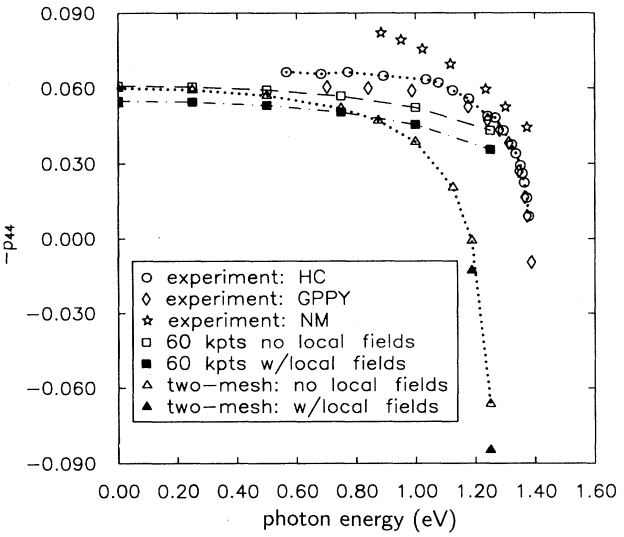

FIG. 6. Best results (two-mesh method) for the frequency-dependent $-p_{44}$ component of the photoelastic tensor with and without local-field effects, contrasted with underconverged (60 k-point density) results and compared to three sets of experimental results. These results are similar to those for the $p_{12}-p_{11}$ (Fig. 5) and $p_{11}+2p_{12}$ (Fig. 7) components in that the dispersion is greatly enhanced when Γ-point corrections are correctly handled. The p_{44} component is similar to $p_{11}+2p_{12}$ and unlike $p_{12}-p_{11}$ in that there is very little change in the static limit when the Γ-point region is correctly integrated. The experimental references are as follows: HC (Ref. 40), GPPY (Ref. 64), and NM (Ref. 65).

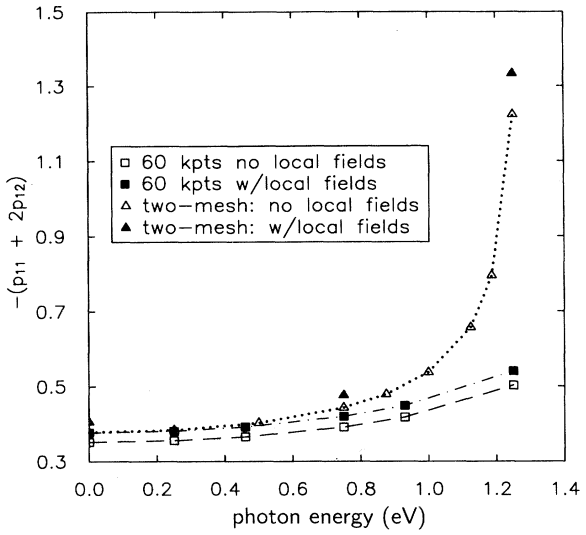

FIG. 7. Best results (two-mesh method) for the frequency-dependent $p_{11}+2p_{12}$ component of the photoelastic tensor (corresponding to hydrostatic strain) with and without local-field effects, contrasted with underconverged (60 k-point density) results. The 60 k-point density—60 k points in the irreducible zone with full cubic symmetry—is sufficient to converge the unstrained dielectric function to within 1%. This and the previous two figures demonstrate the dramatic role played by the Γ-point contributions.

Fig. 5. The results obtained using the 60- and 110-point special k point sets do not even give the correct qualitative behavior; the dispersion is too flat and there is no isotropic point (i.e., a frequency at which the photoelastic tensor vanishes and the dielectric tensor becomes isotropic). In addition, the two uniform meshes (60 and 110 special points) produced a static value 50% larger than the two-mesh result. The change upon convergence is seen to be entirely due to the improved treatment of the Γ-point region (see Fig. 3). These results demonstrate the

TABLE I. Convergence study of the $p_{11}-p_{12}$ component of the photoelastic tensor showing very slow convergence using conventional special k-point methods; especially poor is the value for $\hbar\omega=1.25$ eV. The number of k points for each entry is the equivalent number of points in the irreducible Brillouin zone with full cubic symmetry. The entry designated two-mesh was obtained using our approach utilizing spherical meshes near $k=0$ in combination with a dense (1012 points) uniform mesh. The $k=0$ region is extremely important for the correct description of the dispersion.

Number of k points in irreducible zone	$\hbar\omega=0$	$\hbar\omega=1.25$ eV
60	0.0571	0.0230
110	0.0575	0.0175
182	0.0517	0.0001
280	0.0515	−0.0045
1012	0.0424	−0.0587
two-mesh	0.0382	−0.1799

effectiveness of our approach, in which convergence is achieved once the radial function $\rho(k)$ is converged throughout the zone. In contrast, the special k point method yields results that give the appearance of convergence—hardly changing when the mesh density is increased—yet are, in fact, underconverged.

The slow convergence of $p_{12}-p_{11}$ obtained using special points is illustrated in Table I. Upon increasing the density from 60 to 110 points, significant changes result only for the highest frequencies. In fact, even at the uniform-mesh (special point) density used in the two-mesh method (1012 points), the static value is still overestimated by roughly 11%. Contributions from the small-k region become more important as the frequency is increased, and are seen as the source of the dispersion. The slow convergence obtained using special points is a symptom of the fact that the localized features of the integrand, as illustrated in Figs. 1–3, are inaccurately sampled even by a dense mesh of special points.

The results for the p_{44} component, plotted in Fig. 6, show similarities to those for $p_{12}-p_{11}$. The underconverged results are too flat and have no isotropic point; when converged, the small-k part of the zone makes its greatest impact for the largest frequencies, leading to a better qualitative description of the dispersion. One notable difference, however, concerns the static value—almost no change is obtained upon convergence. The agreement between the converged result for the static value of p_{44} and that obtained using special points is fortuitous, and is due to cancellations of errors.

The last independent component of the photoelastic tensor, $p_{11}+2p_{12}$, is plotted in Fig. 7; unfortunately no frequency-dependent measurements were available for comparison. Table II reports a measurement of the static $p_{11}+2p_{12}$ component. As was the case for p_{44}, little change in the static value is obtained when the two-mesh method is used for the same reasons: cancellation of errors. As before, the dispersion is greatly altered using the two-mesh method.

TABLE II. Summary of the LDA results for the dielectric function and the three independent components of the photoelastic tensor, calculated using 60 special k points, with and without local-field correlations compared with the corresponding self-energy-corrected quantities and experimental results. The local-field effects and self-energy corrections both change the dielectric function in the same way, improving the agreement with experiment, whereas for the photoelastic tensor only self-energy corrections tend to improve the agreement with experiment while local-field corrections worsen the agreement. There are no experimental static values for $p_{12}-p_{11}$ and p_{44}, so the experimental results listed are the values for the lowest measured photon energy: 0.056 eV.

	$\Delta=0$ No loc fields	$\Delta=0$ Loc fields	$\Delta=0.8$ eV No loc fields	$\Delta=0.8$ eV Loc fields	Expt.
ε	13.49	14.17	11.51	10.97	10.92[a]
$p_{12}-p_{11}$	0.027	0.016	0.057	0.047	0.058[b]
$-p_{44}$	0.048	0.042	0.061	0.055	0.066[b]
$p_{11}+2p_{12}$	0.42	0.45	0.35	0.38	0.2[a]

[a]Reference 62.
[b]Reference 40.

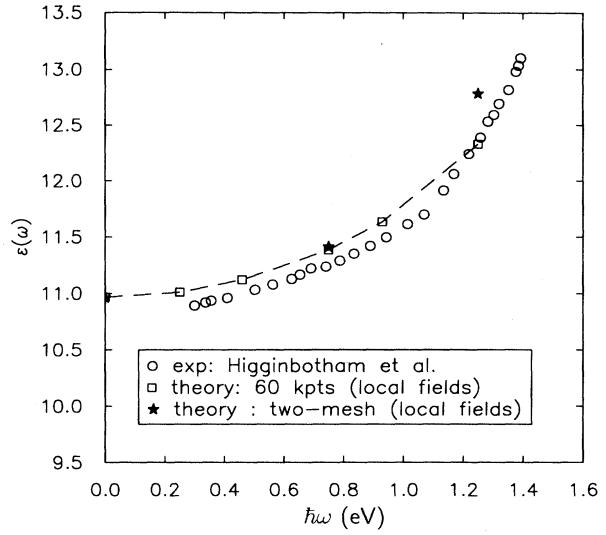

FIG. 8. Results for the frequency-dependent unstrained dielectric function with local-field effects, demonstrating k-point convergence with 60 k points, compared with experimental measurements. The results designated as two mesh are produced using this integration approach, which was required in order to converge the photoelastic tensor. A slight improvement in frequency dispersion is obtained with the two-mesh technique, representing roughly a 4% increase in the dielectric function at $\hbar\omega=1.25$ eV, while the static value changes by less than 1%. The experimental results were taken from Ref. 40.

Despite the fact that our method samples the Brillouin zone more efficiently, by providing a sampling mesh which is far more dense in the small-k region than it is throughout the rest of the zone, roughly an order of magnitude more points are required to achieve convergence for the photoelastic tensor than are required to converge the dielectric function. Figure 8 compares the dielectric function for frequencies below the direct gap ($\hbar\omega_{\text{gap}}\approx 1.5$ eV), obtained with the two-mesh method, with experimental measurements and with results obtained with 60 special points. Unlike the photoelastic tensor, the dielectric function is well converged—to within 1% at $\hbar\omega=0$ eV and to within 4% at $\hbar\omega=1.25$ eV—using just 60 k points. The two-mesh method, on the other hand, requires 1893 points, with 881 of these points concentrated in the region $0\leq k\leq 0.35(2\pi/a)$ which represents less than 2% of the volume of the Brillouin zone. Thus the dominant strain-induced changes in the integrand for the dielectric function are associated with states near the zone center.

A. Self-energy corrections

Self-energy corrections Δ are important for obtaining a good qualitative description of the frequency dispersion and the static values for both the dielectric function and the photoelastic tensor. For the photoelastic tensor[47] (dielectric function) the effect of the self-energy correc-

tion can be summarized as follows: increasing Δ increases (decreases) the static value of the photoelastic tensor (dielectric function) and makes it less dispersive by moving the singularity to higher frequencies. This behavior is easily understood by considering the integrands associated with the photoelastic tensor and the dielectric function. Schematically, the contribution to the frequency-dependent integrand for the photoelastic tensor or the dielectric function arising from the lowest-energy transitions is written as[4]

$$\frac{f(\mathbf{k})[E_{\rm gap}(\mathbf{k})+\Delta]}{\{\omega^2-[E_{\rm gap}(\mathbf{k})+\Delta]^2\}E_{\rm gap}^2(\mathbf{k})}\ , \tag{16}$$

where $E_{\rm gap}(\mathbf{k})$ is the direct gap at $\mathbf{k}$, and $f(\mathbf{k})$ represents the associated squared momentum matrix element in the case of the dielectric function or a difference of such squared matrix elements in the case of the photoelastic tensor. Equation (16) implies that changes in the static integrands are of the form

$$\frac{dg(\mathbf{k})}{d\Delta}=-\frac{g(\mathbf{k})}{[E_{\rm gap}(\mathbf{k})+\Delta]}\ , \tag{17}$$

where $g(\mathbf{k})$ represents either the integrand associated with the photoelastic tensor $P(\mathbf{k})$ or the dielectric function $\epsilon(\mathbf{k})$. Contributions from $k=0$ have the largest effect since the energy denominators are the smallest. Equation (17) implies that the $k=0$ contributions are reduced in magnitude with increasing Δ. For the dielectric function, whose integrand is everywhere positive, an overall reduction with increasing Δ is implied. For the photoelastic tensor, whose integrand is negative for small k and positive for larger k, the decrease in the $k=0$ region implied by Eq. (17) results in an overall increase in the static value.[47]

B. Internal-strain relaxation

Our calculated results for the internal-strain-relaxation parameter ζ are in good agreement with other *ab initio* calculations,[48,49] estimates using empirical potentials,[44] and recent experimental measurements.[50] The application of a strain along the [111] direction (trigonal strain)—as is required for the calculation of the p_{44} component of the photoelastic tensor—destroys the equivalence between the tetrahedral bonding directions and allows for a structural relaxation between the two face-centered-cubic (fcc) sublattices which comprise the zinc-blende structure. Kleinman[48,51] defined the internal strain parameter ζ such that $\zeta=0$ corresponds to the situation in which there is no relaxation and all atomic positions are rigidly strained, while $\zeta=1$ corresponds to the situation in which a relaxation occurs such that all of the bond lengths are the same and assume their original unstrained length ($\sqrt{3}a/4$). In terms of this definition, for $\zeta=0$ bond lengths assume the values $(\sqrt{3}a/4)(1+2\eta/3)$ for the strain direction and $(\sqrt{3}a/4)(1-2\eta/6)$ for the other three formerly equivalent directions, where η is the magnitude of the strain.

The strain parameter ζ is defined in terms of the [111] volume-conserving component of the strain as only this (trigonal shear strain) component lowers the symmetry and permits the relaxation. The strain parameter is a fundamental property of the material and characterizes the relative importance of two- and three-body forces. In other words, if only pairwise nearest-neighbor atomic interactions were important then $\zeta=1$ would hold and all bond lengths would be equal. However, in the other extreme limit, if only bond angles were important then $\zeta=-\frac{1}{2}$ would hold and all bond angles would be equal. In general, ζ takes on some intermediate value. In our *ab initio* calculations, ζ is determined by total-energy minimization. The parameter ζ was also estimated analytically using Stillinger-Weber (two- and three-body) empirical potentials by assuming an infinitesimal strain and expanding the potentials about the equilibrium (unstrained) configuration.[44,50–55] The results for this parameter are summarized in Table III. Good agreement with the previous calculations[48,49] and recent experiments[50] is found. Our *ab initio* ζ, presented in Table III, was used in all calculations of p_{44}.[44,55]

TABLE III. Calculated results for the internal strain parameter ζ in comparison with experimental and previous calculations. Our result was calculated by minimizing the total energy with respect to ζ for a strain of magnitude $\delta l/l=0.004$, where l is any length measured along the [111] direction.

Source	ζ
Present work (*ab initio*)	0.517
Present work (empirical)[a]	0.53
Expt.[b]	0.55±0.02
Expt.[c]	0.76
Calc.[d]	0.528
Calc.[e]	0.48
Calc.[f]	0.6

[a]Reference 44.
[b]Reference 50.
[c]Reference 63.
[d]Reference 49.
[e]Reference 48.
[f]Reference 67.

IV. DISCUSSION

The oscillations in the integrand at small k associated with the photoelastic tensor arise from corresponding oscillations in the integrand for the unstrained dielectric function.[44] Using second-order $\mathbf{k}\cdot\mathbf{p}$ theory,[56] we have derived an analytical expression for the integrand associated with the dielectric function, which is expressed as a power series to second order in k. This expression was cast in the form of a spherical-harmonic expansion, and expressions for the expansion coefficients $C_{lm}(k)$ for $l\leq 6$ were extracted.

A fairly simple interpretation for the oscillations in the integrand near $k=0$ has emerged from this analysis: the valence eigenstate of crystal momentum $\mathbf{k}$ is a p orbital aligned along the direction of $\mathbf{k}$ having the spatial dependence

$$\psi_{\mathbf{k}}(\mathbf{r}) \propto \mathbf{k}\cdot\mathbf{r} \ . \tag{18}$$

The squared optical matrix element thus has the k dependence $(\mathbf{k}\cdot\mathbf{p})^2$, where $\mathbf{p}$, the momentum operator, lies along the polarization direction of the incident light field. The angular part of this k dependence can be expressed as a spherical-harmonic expansion using only spherical harmonics of order $l=0$ and 2. The energy bands for small k obey cubic symmetry and therefore can be written as a similar expansion keeping only terms of order $l=0$ and 4. The complete derivation and explicit expressions for the spherical-harmonic coefficients $C_{lm}(k)$ up to $l=6$ are given in Ref. 44.

For $l=4$ and 6 the analytic expressions are simple enough—all proportional—so that comparisons can be made in the form of ratios of the various components. The ratios $C_{lm}/C_{l'm'}$ at $k=0.01(2\pi/a)$, as obtained using the analytical expressions, are compared in Table IV with *ab initio* results. Good agreement is obtained for the higher harmonics, whereas the agreement for the lower harmonics is less satisfactory. This is consistent with the behavior of the spherical-harmonic coefficients for the photoelastic tensor as illustrated in Fig. 2: the larger the value of l the less important are the effects of terms of order k^3 and higher. This follows from the fact that the position of the maximum of $C_{lm}(k)$ moves to larger k with increasing l. Our treatment, which only includes terms to order k^2, and no linear term, cannot be expected to adequately describe $C_{20}(k)$ (Fig. 2) near its maximum.

Comparison of the spherical-harmonic expansion coefficients of the integrand for the dielectric function (Table IV) with those for the photoelastic tensor (Fig. 2) substantiates that the oscillations in the integrand for the photoelastic tensor arise from corresponding oscillations in the dielectric-function integrand. This is further confirmed in Table V, which compares the expansion coefficients of the difference $\varepsilon_{xx}(\mathbf{k})-\varepsilon_{zz}(\mathbf{k})$ in the strained and unstrained crystals [we are assuming strain along the z axis; see Eq. (4)], showing similar oscillations in both situations. Since

$$p_{12}-p_{11} \propto \varepsilon_{xx}-\varepsilon_{zz} \ , \tag{19}$$

we conclude that the oscillations arise not as a result of the strain but are intrinsic to the dielectric function.

TABLE IV. Comparison of analytical [using second-order $\mathbf{k}\cdot\mathbf{p}$ theory (Refs. 44 and 56)] and *ab initio* results for the spherical-harmonic coefficients of the integrand associated with the $\{xx\}$ component of the unstrained long-wave static dielectric function at $k=0.01(2\pi/a)$. Comparisons are presented as ratios of the various coefficients. All ratios are of the same order of magnitude, indicating that the analytical treatment gives an accurate description of the qualitative features of the small-k integrand. The ratios for most of the $l=6$ coefficients are in excellent agreement, indicating that terms of order k^3 and higher are small for these coefficients. The discrepancies for the lower-l coefficients indicate that terms of order k^3 and possibly higher are not negligible, as can also be inferred from Fig. 2 (the low-l coefficients in Fig. 2 have maxima for small k, indicating the importance of higher-order powers in k).

	$\mathbf{k}\cdot\mathbf{p}$ (analytical)	Calculated
$\lvert C_{40}/C_{42}\rvert$	7.50	1.43
$\lvert C_{40}/C_{44}\rvert$	1.43	0.89
$\lvert C_{44}/C_{42}\rvert$	5.23	1.60
$\lvert C_{60}/C_{40}\rvert$	0.10	0.02
$\lvert C_{60}/C_{62}\rvert$	1.42	1.42
$\lvert C_{60}/C_{64}\rvert$	3.79	5.28
$\lvert C_{60}/C_{66}\rvert$	0.93	0.96
$\lvert C_{62}/C_{64}\rvert$	2.70	3.73
$\lvert C_{62}/C_{66}\rvert$	0.66	0.67
$\lvert C_{62}/C_{66}\rvert$	0.24	0.18

TABLE V. Spherical-harmonic expansion coefficients for the difference $\{xx\}-\{zz\}$ of the components of the integrand associated with the static, long-wave dielectric function at $k=0.01(2\pi/a)$ (the experimental lattice constant $a=10.6807$ a.u.), with and without strain. This difference is relevant to the eigenvalue of the photoelastic tensor under [001] strain $p_{12}-p_{11}$, since $p_{12}-p_{11} \propto \varepsilon_{zz}-\varepsilon_{xx}$. These results were numerically projected from the results of *ab initio* calculations. The first column gives the unstrained results, while the second presents those obtained under strain. The C_{00} coefficient (which is the only one which contributes to the integral) becomes nonzero under strain yet remains at least an order of magnitude smaller than some of the higher-l coefficients.

Coefficient	$xx-zz$ (unstrained)	$xx-zz$ ([001] strain)
C_{00}	0.0	−2007.6
C_{20}	15 110.8	15 200.1
C_{40}	64.1	57.6
C_{44}	−53.7	−53.1
C_{60}	−3.9	−4.0
C_{64}	−1.0	−1.0

A. Comparison with experiment

Figures 5 and 6 demonstrate that while the improved calculation yields better qualitative agreement with experiment for the frequency dispersion of the photoelastic tensor, the quantitative agreement is less than satisfactory. In a previous calculation for Si, the less-than-satisfactory dispersion of the photoelastic tensor near the lowest direct gap in Si[28] may have resulted from inadequate k-point sampling. Si is qualitatively different, however, in that the lowest-energy transitions at Γ are forbidden in Si; the allowed transitions at Γ are higher in energy than the average band gap and are thus suppressed (by the energy denominators) compared to other transitions. Thus, unlike the small-direct-gap material GaAs, in which transitions near the Γ point dominate the dispersion, the dispersion in Si cannot be attributed to a single region in k space. This disparity between direct- and indirect-gap materials is not limited to Si and GaAs.[56–59]

For GaAs as well as Si the self-energy-corrected results are greatly improved over the LDA ($\Delta=0$) results (see Table II); the LDA predicts static values for the photoelastic tensor (dielectric function) which are too low (too high) by roughly 10% (30%) and the singularity in the frequency dispersion is too low in energy. The photoelastic tensor is far more sensitive to Δ than is the dielectric function—a direct consequence of the increased importance of the region near $k=0$ for the photoelastic tensor.

While $\Delta=0.8$ eV gave excellent results for the frequency dependence of the dielectric function (see Fig. 8), the frequency dependence for the photoelastic tensor calculated with $\Delta=0.8$ eV—the gap suggested by *GW* calculations[25]—is slightly too dispersive (compare Figs. 5 and 6), and $\Delta=0.94$ eV—the Δ which aligns the $k=0$ with the experimental gap—yields a slight improvement in the dispersion.

Local fields give rise to substantial corrections for both the dielectric function and the photoelastic tensor but, while the dielectric function improves in comparison to experiment, the photoelastic tensor worsens (see Table II). Local fields improve the dielectric function by reducing it by roughly 5% over the LDA, yielding agreement to within a few percent of the experiments over the entire frequency range below the direct band gap. These frequency-insensitive corrections are, however, fairly sensitive to the strain state of the crystal, as can be seen in Figs. 6 and 7; there would be no local-field corrections to the photoelastic tensor if each component of the dielectric function had the same local-field correction in the presence of strain. In both cases for which experimental results exist—p_{44} (Fig. 6) and $p_{12}-p_{11}$ (Fig. 5)—the effect of local fields is to worsen the agreement with experiments by roughly 5%, with the magnitude of the correction becoming slightly larger as the band gap is approached.

Our results for the photoelastic tensor in GaAs, while converged within our one-electron theory, are less satisfactory in comparison with experiment than we have come to expect (agreement to within a few percent[4]), indicating that effects outside of our theory such as spin-orbit, particle-hole, and thermal effects may be significant. In light of recent calculations for the photoelastic effect in Si,[28] it seems unlikely that the inclusion of particle-hole (exciton) and thermal effects will improve the agreement with experiment. In Ref. 28 it was argued that excitonic effects and thermal effects could be crudely modeled by reducing the self-energy correction by one to two tenths of an electron volt. A reduction in the self-energy correction Δ reduces the static value and makes the frequency dependence more dispersive. In the Si calculation the results were slightly too high and less dispersive than the measurements implying that a reduction in the self-energy correction would improve the results. For GaAs, however, we are faced with the opposite situation and a reduction of the self-energy correction would worsen the agreement with the data.

Spin-orbit effects hold more promise for reducing the discrepancies with experiment. The derivation of the energies and wave functions near $k=0$ using $\mathbf{k}\cdot\mathbf{p}$ theory has been carried out both with and without the inclusion of spin orbit.[44] The integrands for the dielectric function and the photoelastic tensor are altered significantly in two ways: (1) inclusion of spin orbit alters the symmetry of the Hamiltonian resulting in strain-induced contributions to the matrix elements; and (2) the energy denominators are shifted—one band shifts downward in energy by $2\Delta_{so}/3$ and the other two bands shift upward by $\Delta_{so}/3$, where $\Delta_{so}=0.34$ eV is the experimental spin-orbit splitting.[61]

Estimates made using the $\mathbf{k}\cdot\mathbf{p}$ energies and wave functions indicate that the magnitude of the $k=0$ integrand for the dielectric tensor is reduced by 24%, and the integrand for the photoelastic tensor is reduced to 40% when spin orbit is included.[44] A crude estimate of this effect on the entire integral would be to assume the Γ contribution to each integral to be equal to the difference between the two-mesh result and the 60-point result. The static 60-point result for $p_{12}-p_{11}$ was roughly 50% larger than the two-mesh result, as illustrated in Fig. 5. Assuming this difference to be reduced by 40% upon including spin orbit implies that the photoelastic tensor component $p_{12}-p_{11}$ would be increased by 20%. For the dielectric function, the Γ-point contribution is only on the order of 1%, so the overall effect of including spin orbit at $k=0$ is to increase the static dielectric constant by less than 0.25% over the two-mesh static value.

V. SUMMARY

We have presented results of calculations of the photoelastic tensor for photon energies below the fundamental band gap in GaAs. A numerical problem has been solved which arose out of the need to accurately perform Brillouin-zone integrations over functions which are oscillatory in the angle $\hat{k}$ and sharply peaked as a function of the magnitude k near the Γ point. Traditional special k-point methods were found to be inadequate to sample this very important region. An integration approach has been presented which overcomes the numerical difficulties and leads to a dramatic improvement in the qualitative frequency dispersion of the photoelastic tensor in comparison with experiment despite a 50% shift of $p_{12}-p_{11}$ away from the measurement. These large corrections are seen to come almost entirely from a small neighborhood of the $k=0$ point which comprises less than 2% of the zone volume.

The energy bands and wave functions near $k=0$ have been investigated using second-order $\mathbf{k}\cdot\mathbf{p}$ theory, demonstrating that the angular oscillations associated with the photoelastic integrand are directly related to corresponding oscillations in the integrand for the dielectric function. While inclusion of spin orbit seems promising for reducing the discrepancies between theory and experiment, it is argued that particle-hole and thermal effects would tend to worsen the agreement with experiment. Self-energy corrections and local-field effects were shown to have a significant effect on the results.

In summary, we have shown that the photoelastic tensor in GaAs is extremely sensitive to details of the electronic structure near $k=0$ and as such should provide a stringent test for improvements to electronic structure theory.

ACKNOWLEDGMENTS

We are grateful to W. Aulbur, M. Alouani, and D. Cox for helpful discussions. We would especially like to thank D. Allan and M. Teter of Corning Inc. for allowing us to use their band structure code. This work was supported by DOE–Basic Energy Sciences, Division of Materials Sciences, the Natural Science Foundation, and the Ohio Supercomputer Center.

*Present address: Physics Department, General Motors Research and Development Center, Warren, MI 48090-9055.

†Present address: Bldg. 221/A253, NIST, Gaithersburg, MD 20899.

[1]For a review, see *Strained-Layer Superlattices: Physics,* edited by T. Pearsall, Semiconductors and Semimetals Vol. 32 (Academic, New York 1990); *Strained-Layer Superlattices: Materials Science and Technology,* edited by T. Pearsall (Academic, New York, 1991).

[2]G. C. Osbourn, J. Appl. Phys. **53**, 1586 (1982).

[3]H. Temkin, T. P. Pearsall, J. C. Bean, R. A. Logan, and S. Luryi, Appl. Phys. Lett. **48**, 330 (1986).

[4]Z. H. Levine and D. C. Allan, Phys. Rev. Lett. **63**, 1719 (1989); **66**, 41 (1991); Phys. Rev. B **43**, 4187 (1991); **44**, 12 781 (1991); **48**, 14 768(E) (1993).

[5]S. Baroni, P. Giannozzi, and A. Testa, Phys. Rev. Lett. **58**, 1861 (1987).

[6]X. Gonze, D. C. Allan, and M. P. Teter, Phys. Rev. Lett. **68**, 3603 (1992).

[7]S. Baroni and R. Resta, Phys. Rev. B **33**, 7017 (1986).

[8]M. Alouani, L. Brey, and N. E. Christensen, Phys. Rev. B **37**, 1167 (1988).

[9]R. Resta and K. Kunc, Phys. Rev. B **34**, 7146 (1986).

[10]W. R. L. Lambrecht and B. Segall, Phys. Rev. B **40**, 40 (1989).

[11]S. G. Louie, J. R. Chelikowsky, and M. L. Cohen, Phys. Rev. Lett. **62**, 2853 (1989).

[12]W. Hanke and L. J. Sham, Phys. Rev. B **21**, 4656 (1980).

[13]G. E. Engel and B. Farid, Phys. Rev. B **46**, 15 812 (1982).

[14]J. P. Walter and M. L. Cohen, Phys. Rev. B **2**, 1821 (1970).

[15]C. S. Wang and B. M. Klein, Phys. Rev. B **24**, 3417 (1981).

[16]A. Dal Corso, S. Baroni, and R. Resta, Phys. Rev. B **49**, 5323 (1994).

[17]X. Gonze, Ph. Ghosez, and R. W. Godby (unpublished).

[18]P. Hohenberg and W. Kohn, Phys. Rev. **136**, B864 (1964).

[19]W. Kohn and L. J. Sham, Phys. Rev. **140**, A1133 (1965).

[20]R. M. Dreizler and E. K. U. Gross, *Density Functional Theory: An Approach to the Quantum Many-Body Problem* (Springer-Verlag, New York, 1990).

[21]R. O. Jones and O. Gunnarsson, Rev. Mod. Phys. **61**, 689 (1989).

[22]U. von Barth and A. R. Williams, in *Theory of the Inhomogeneous Electron Gas,* edited by S. Lundqvist and N. H. March (Plenum, New York, 1983), p. 189.

[23]M. S. Hybertsen and S. G. Louie, Phys. Rev. B **34**, 5390 (1986).

[24]M. S. Hybertsen and S. G. Louie, Phys. Rev. B **38**, 4033 (1988).

[25]R. W. Godby, M. Schlüter, and L. J. Sham, Phys. Rev. B **37**, 10 159 (1988).

[26]J. F. Nye, *Physical Properties of Crystals* (Clarendon, Oxford, 1989).

[27]G. L. Bir and G. E. Pikus, *Symmetry and Strain-Induced Effects in Semiconductors* (Wiley, New York, 1974).

[28]Z. H. Levine, H. Zhong, S. Wei, D. C. Allan, and J. W. Wilkins, Phys. Rev. B **45**, 4131 (1992).

[29]D. C. Allan and M. P. Teter, Phys. Rev. Lett. **59**, 1136 (1987).

[30]M. P. Teter, M. C. Payne, and D. C. Allan, Phys. Rev. B **40**, 12 255 (1989).

[31]D. R. Hamann, Phys. Rev. B **40**, 2980 (1989).

[32]L. Kleinman and D. M. Bylander, Phys. Rev. Lett. **48**, 1425 (1982).

[33]M. P. Teter (unpublished). With this parametrization, the exchange-correlation potential is differentiable with respect to density at all densities.

[34]D. M. Ceperley and B. J. Alder, Phys. Rev. Lett. **45**, 566 (1980).

[35]H. J. Monkhorst and J. D. Pack, Phys. Rev. B **13**, 5188 (1976).

[36]D. J. Chadi and M. L. Cohen, Phys. Rev. B **8**, 5747 (1973).

[37]S. L. Adler, Phys. Rev. **126**, 413 (1962); N. Wiser, *ibid.* **129**, 62 (1963).

[38]M. H. Grimsditch, E. Kisela, and M. Cardona, Phys. Status Solidi A **60**, 135 (1980).

[39]Thus we write $p_{\alpha\beta}=p_{ijkl}$, where α and β correspond to the pairs ij and kl. The shorthand notation for the strain tensor μ is slightly different: ($\mu_{ij}=\mu_\alpha, \alpha=1$, 2, and 3) and ($2\mu_{ij}=\mu_\alpha$, $\alpha=4$, 5, and 6).

[40]C. W. Higginbotham, M. Cardona, and F. H. Pollak, Phys. Rev. **184**, 821 (1969).

[41]A spherical-harmonic integration mesh, which correctly satisfies the orthogonality relation Eq. (8) is constructed at a given radius in k space by placing points on a sphere as follows. The k_z coordinates are chosen to exactly integrate the Legendre polynomials (Ref. 68), $P_l(k_z/k)$ for all $l<2l_{\max}$, where $l_{\max}$ is the highest value of l for which Eq. (8) is satisfied. The k_x and k_y coordinates are then chosen such that, for each k_z, there are $2l_{\max}$ equally spaced points on the circle of radius $k\sin(\cos^{-1}(k_z/k))$. The mesh is constructed in this way since the product of two spherical harmonics in Eq. (8) factors into a product of a Legendre polynomial (dependent only on k_z/k), and an azimuthal part which depends only on k_x and k_y through the azimuthal angle ϕ as $e^{im\phi}$ where ϕ is the usual azimuthal angle of the vector $\mathbf{k}$ in spherical-polar coordinates: $\mathbf{k}=(k,\theta,\phi)$. Having $2l_{\max}$ uniformly spaced points in ϕ allows one to exactly integrate $e^{im\phi}$ for all $m<2l_{\max}$ (Ref. 68).

[42]An explicit expression can be obtained for $\tilde{P}(\mathbf{k})$, in terms of the values of the sampled integrand as

$$\tilde{P}(\mathbf{k})=\frac{1}{N}\sum_{\mathbf{k}_j\in\{\mathbf{k}^{\text{large}}\}}P(\mathbf{k}_j)\prod_{\sigma=x,y,z}\left[\cos[N\pi(k_\sigma-k_{j\sigma})/2]+\frac{\sin[(N-1)\pi(k_\sigma-k_{j\sigma})/2]}{\sin[\pi(k_\sigma-k_{j\sigma})/2]}\right],$$

where $\mathbf{k}^{\text{large}}$ is a uniform mesh of points spanning the first and second Brillouin zones (if only points in the first zone were used, spurious nodes would appear between sampling points) (Ref. 44). The above equation is obtained by analytically summing over the direct-space vectors (Ref. 44).

[43]This functional form was proposed by Steve White (private communication).

[44]J. E. Raynolds, Ph.D. dissertation, Ohio State University, 1994.

[45]For the section between $k=0$ and 0.01 a quadratic interpolation of the radial function is assumed. An integration point is placed at $k=0$ to obtain the second derivative $d^2\rho(k)/dk^2|_{k=0}$ of the radial function to determine the coefficient of the quadratic term.

[46]For the tetragonal and trigonal symmetries, corresponding to strain along [001] and [111], used to compute the $p_{12}-p_{11}$ and p_{44} components of the photoelastic tensor, respectively, the corresponding numbers of k points are 3664 and 4852, respectively. The radial function is integrated using Simpson's rule for $0.01\le k\le 0.35$ (see Fig. 3). For the section between $k=0$ and 0.01 a quadratic interpolation of the radial function is assumed. In practice we arrive at a collection of points and weights which are read by our optical-response program.

[47]For this particular example, we have the $p_{12}-p_{11}$ component

in mind. We will often refer to this component since it is the most sensitive to the details of the states near $k=0$. With regard to the present example, $-p_{44}$ behaves qualitatively like $p_{12}-p_{11}$, and $p_{11}+p_{12}$ behaves in the opposite way.

[48]O. H. Nielsen and R. M. Martin, Phys. Rev. B **32**, 3792 (1985).

[49]S. de Gironcoli, S. Baroni, and R. Resta, Phys. Rev. Lett. **62**, 2853 (1989).

[50]C. S. G. Cousins, L. Gerward, J. Staun Olsen, B. Selsmark, B. J. Shedlon, and G. E. Webster, J. Semicond. Sci. Technol. **4**, 333 (1989).

[51]L. Kleinman, Phys. Rev. **128**, 2614 (1962).

[52]F. H. Stillinger and T. A. Weber, Phys. Rev. B **31**, 5262 (1985).

[53]G. A. Weber and F. H. Stillinger, Phys. Rev. B **32**, 5402 (1985).

[54]Z. Q. Wang and D. Stroud, Phys. Rev. B **42**, 5353 (1990).

[55]S. Wei, D. C. Allan, and J. W. Wilkins, Phys. Rev. B **46**, 12 411 (1992).

[56]E. O. Kane, in *Physics of III-V Compounds,* edited by R. K. Willardson and A. C. Beer, Semiconductors and Semimetals Vol. 1 (Academic, New York, 1966).

[57]A. N. Pikhtin and A. D. Yas'kov, Fiz. Tekh. Poluprovodn. **22**, 969 (1988) [Sov. Phys. Semicond. **22**, 613 (1988)].

[58]S. A. Geidur and A. D. Yas'kov, Opt. Spektrosk. **57**, 74 (1984) [Opt. Spectrosc. (USSR) **57**, 45 (1984)].

[59]A. N. Pikhtin and A. D. Yas'kov, Fiz. Tekh. Poluprovodn. **12**, 1047 (1978) [Sov. Phys. Semicond. **1**, 622 (1978)].

[60]M. DiDomenico, Jr. and S. H. Wemple, J. Appl. Phys. **40**, 720 (1969); **40**, 735 (1969); Phys. Rev. Lett. **23**, 1156 (1969); Phys. Rev. B **1**, 193 (1970); **3**, 1338 (1971).

[61]F. H. Pollak and M. Cardona, Phys. Rev. **172**, 816 (1968).

[62]A. R. Goñi, K. Syassen, and M. Cardona, Phys. Rev. B **41**, 10 104 (1990).

[63]C. N. Koumelis, G. E. Zardas, C. A. Londos, and D. K. Leventuri, Acta Crystallogr. Sect. A **32**, 84 (1975).

[64]S. A. Geidur, A. N. Pikhtin, V. T. Prokopenko, and A. D. Yaskov, Opt. Spektrosk. **46**, 714 (1979) [Opt. Spectrosc. (USSR) **46**, 399 (1979)].

[65]V. I. Nikitenko and G. P. Martynenko, Fiz. Tverd. Tela (Leningrad) **7**, 622 (1965) [Sov. Phys. Solid State **7**, 494 (1965)].

[66]A. Feldman and D. Horowitz, J. Appl. Phys. **39**, 5597 (1968).

[67]P. Etchegoin, J. Kircher, M. Cardona, C. Grein, and E. Bustarret, Phys. Rev. B **46**, 15 139 (1992).

[68]*Handbook of Mathematical Functions,* edited by M. Abramowitz and I. A. Stegun, Natl. Bur. Stand. (U.S.) Appl. Math. Ser. No. 55 (U.S. GPO, Washington, DC, 1968; reprinted by Dover Publications, New York, 1970), pp. 916–919; K. E. Atkinson, *An Introduction to Numerical Analysis* (Wiley, New York, 1978), pp. 250–253.